1 **Landfast ice thickness in the Canadian Arctic Archipelago from Observations and Models**

2 Stephen. E. L. Howell[1], Frédéric Laliberté[1], Ron Kwok[2], Chris Derksen[1] and Joshua King[1]

3 [1]Climate Research Division, Environment Canada, Toronto, Canada

4 [2]Jet Propulsion Laboratory, California Institute of Technology, Pasadena, California, USA

5 **Abstract**

6 Observed and modelled landfast ice thickness variability and trends spanning more than five

7 decades within the Canadian Arctic Archipelago (CAA) are summarized. The observed sites

8 (Cambridge Bay, Resolute, Eureka and Alert) represent some of the Arctic's longest records of

9 landfast ice thickness. Observed end-of-winter (maximum) trends of landfast ice thickness

10 (1957-2014) were statistically significant at Cambridge Bay (-4.31±1.4 cm decade$^{-1}$), Eureka (-

11 4.65±1.7 cm decade$^{-1}$) and Alert (-4.44±1.6 cm decade$^{-1}$) but not at Resolute. Over the 50+ year

12 record, the ice thinned by ~0.24-0.26 m at Cambridge Bay, Eureka and Alert with essentially

13 negligible change at Resolute. Although statistically significant warming in spring and fall was

14 present at all sites, only low correlations between temperature and maximum ice thickness were

15 present; snow depth was found to be more strongly associated with the negative ice thickness

16 trends. Comparison with multi-model simulations from Coupled Model Intercomparison project

17 phase 5 (CMIP5), Ocean Reanalysis Intercomparison (ORA-IP) and Pan-Arctic Ice-Ocean

18 Modeling and Assimilation System (PIOMAS) show that although a subset of current generation

19 models have a 'reasonable' climatological representation of landfast ice thickness and

20 distribution within the CAA, trends are unrealistic and far exceed observations by up to two

21 orders of magnitude. ORA-IP models were found to have positive correlations between

22 temperature and ice thickness over the CAA, a feature that is inconsistent with both observations

23 and coupled models from CMIP5.

**1. Introduction**

The World Meteorological Organization (WMO, 1970) defines landfast sea ice as "sea ice which remains fast along the coast, where it is attached to the shore, to an ice wall, to an ice front, or over shoals, or between grounded icebergs." In the Arctic, this ice typically extends to the 20-30 m isobaths [*Mahoney et al.,* 2007; *Mahoney et al.,* 2014]. It melts each summer and reforms in the fall but there are regions along the northern coast of the Canadian Arctic Archipelago (CAA) where multi-year landfast ice (also termed an "ice plug") is present. The two most prominent regions of multi-year landfast sea ice in the CAA are located in Nansen Sound and Sverdrup Channel [*Serson*, 1972; *Serson*, 1974] (Figure 1). It has been documented that ice remained intact from 1963-1998 in Nansen Sound and from 1978-1998 in Sverdrup Channel [*Jeffers et al.,* 2001; *Melling*, 2002; *Alt et al.,* 2006]. The extreme warm year of 1998 disintegrated the ice in both regions and their survival during the summer melt season in recent years has occurred less frequently [*Alt et al.*, 2006]. Over the entire Arctic, landfast ice extent is declining at 7% decade$^{-1}$ since the mid-1970s [*Yu et al.,* 2013]

Records of landfast ice thickness provide annual measures of ice growth that can also almost entirely be attributed to atmospheric forcing with negligible deep ocean influence on local ice formation. While the key forcings on landfast ice and offshore ice are different, the seasonal behavior of landfast ice can nevertheless provide useful information for understanding the interannual variability of ice thickness in both regimes. Presently, there is no pan-Arctic network for monitoring changes in landfast ice but available measurements suggest thinning in recent years. Thickness measurements near Hopen, Svalbard revealed thinning of landfast ice in the Barents Sea region by 11 cm decade$^{-1}$ between 1966 and 2007 [*Gerland et al.,* 2008]. From a composite time series of landfast ice thickness from 15 stations along the Siberian coast,

47    *Polyakov et al.* [2010] estimate an average rate of thinning of 3.3 cm decade$^{-1}$ between the mid-

48    1960s and early 2000s. Relatively recent observations by *Mahoney et al.* [2007] and

49    *Druckenmiller et al.* [2009] found longer ice-free seasons and thinner landfast ice compared to

50    earlier records.

51        At four sites in the CAA, *Brown and Cote* [1992] (hereinafter, BC92) provided the first

52    examination of the interannual variability of end-of-winter (maximum) landfast ice thickness and

53    associated snow depth over the period 1957-1989. Their results highlighted the insulating role of

54    snow cover in explaining 30-60% of the variance in maximum ice thickness. Similar results were

55    also reported by *Flato and Brown* [1996] and *Gough et al.* [2004]. In the record examined by

56    BC92, no evidence for systematic thinning of landfast ice in the CAA was found. Landfast ice

57    thickness records at several of these CAA sites are now over 50 years in length, which represents

58    an addition of more than two decades of measurements since BC92 during a period that saw

59    dramatic reductions in the extent and thickness of Arctic sea ice [e.g. *Kwok and Rothrock*, 2009;

60    *Stroeve et al.,* 2012].

61        The sparse network of long term observations of snow and ice thickness in the Arctic

62    (clearly exhibited by only four ongoing measurements sites operated by Environment Canada in

63    the CAA) has made the use of models imperative to provide a broader regional scale perspective

64    of sea ice trends in a warming climate. Given the coarse spatial resolution of global climate

65    models, previous studies focusing on the CAA have relied on either a one-dimensional

66    thermodynamic dynamic model [*Flato and Brown*, 1996; *Dumas et al.,* 2006] or a regional three-

67    dimensional ice-ocean coupled model [e.g. *Sou and Flato*, 2009]. Specifically, *Dumas et al.*

68    [2006] found projected maximum ice thickness decreases of 30 cm by 2041-2060 and 50 cm by

69    2081-2100 and *Flato and Sou* [2009] reported a potential 17% decrease in overall ice thickness

70  throughout the CAA by 2041-2060. However, in recent years some global climate models,

71  reanalysis products, and data assimilation systems are now of sufficient spatial resolution to

72  assess potential landfast ice thickness changes within the CAA.

73       This analysis examines the trends of measured landfast ice thickness, snow depth and air

74  temperature over a 50+ year period between 1957 and 2014 and compares the results with the

75  earlier analysis by BC92. We then use this observational foundation to evaluate the

76  representativeness of landfast ice in state-of-the-art global climate models, assimilation systems

77  and re-analysis products.

78

79  **2. Data Description**

80  **2.1. Observations**

81       Landfast ice thickness and corresponding snow depth measurement have been made

82  regularly at many coastal stations throughout Canada since about 1950. These data are quality

83  controlled and archived at the Canadian Ice Service (CIS) and represent one of the few available

84  sources of continuous ice thickness measurements in the Arctic. In general, thickness

85  measurements are taken once per week, starting after freeze-up when the ice is safe to walk on

86  and continuing until breakup or when the ice becomes unsafe. Complete details of this dataset

87  are provided by Brown and Cote (1992). The dataset is available on the CIS web site

88  (http://www.ec.gc.ca/glaces-ice/, see Archive followed by Ice Thickness Data). Four sites in the

89  CAA were selected for study: Alert, Eureka, Resolute, and Cambridge Bay (Figure 1). Although

90  there are other sites in the database, these sites are the only ones than span the same 55-year

91  period between 1960 and 2014. The record at Mould Bay, used in BC92, terminated in the early

92  1990s. Together these sites cover ~20° in latitude (Figure 1) that are adjacent to an area of thick

93    Arctic sea ice that experienced the highest thinning in recent years [*Kwok and Rothrock*, 2009;

94    *Laxon et al.*, 2013]. Values of maximum or end-of-winter ice thickness and corresponding snow

95    depth during the ice growth season were extracted from the weekly ice and snow thickness data

96    at the selected sites (see supplementary material). As this study is concerned with annual

97    variability in maximum ice thickness, the main period of interest extends from September to late

98    May.

99         The other source of observed data used in this study was Environment Canada's monthly

100   mean air temperature records at Alert, Eureka, Resolute, and Cambridge Bay for which a

101   complete description is provided by *Vincent et al.* [2012].

102

103   **2.2. Models**

104        The representation of CAA landfast sea ice thickness within the Coupled Model

105   Intercomparison project phase 5 (CMIP5) is analyzed using the 1850-2005 Historical experiment

106   followed by the 2006-2099 Representative Concentration Pathway 8.5 (RCP85) experiment

107   [*Taylor et al.*, 2012] (Table 1). Monthly sea ice thickness (variable *sit*), sea ice concentration

108   (variable *sic*), 2 meter temperature (variable *tas*) and snow depth (variable *snd*) were used. The

109   CMIP5 data were retrieved from the British Atmospheric Data Centre database and accessed

110   through the Center for Environmental Data Analysis (www.ceda.ac.uk). Ensemble r6i1p1 and

111   r7i1p1 from model EC-EARTH were removed because of corrupted data. We obtain the multi-

112   model mean of trends and their statistical significance at each grid point by creating the

113   distribution of trends through a Monte-Carlo simulation. We use a t-distribution for the

114   interannual variability and build a noise model to account for internal variability as in *Swart et*

115   *al.* [2014] and *Laliberté et al.* [2016]. We obtain the multi-model mean of Pearson correlations

116    and their statistical significance by first performing a Fisher transform and then applying the

117    same method as for the trends. The inverse Fisher transform is applied after obtaining the multi-

118    model mean and its significance. See the appendix for a complete description of the method.

119         We also investigate ice thickness values from a selection of the highest resolution models

120    [*Storto et al.,* 2011; *Forget et al.,* 2015; *Haines et al.,* 2014, *Zuo et al.,* 2015; *Masina et al.,*

121    2015] from the Ocean Reanalysis Intercomparison (ORA-IP) [*Balsameda et al.,* 2015; *Chevallier*

122    *et al.,* 2016] (Table 2) and from the Pan-Arctic Ice-Ocean Modeling and Assimilation System

123    (PIOMAS) [*Zhang and Rothrock*, 2003]. Supporting 2 meter temperature data was obtained from

124    ERA-Interim [*Dee et al.,* 2011].

125

126    **3. Results and Discussion: Observations**

127    **3.1. Climatology**

128         The average behavior of landfast ice at the four sites over the 50+ year record is

129    summarized in Table 3. Ice growth, approximately linear through most of the season, slows after

130    March (Figure 2). Ice thickness reaches a maximum of ~2-2.3 m by late May at all sites. Values

131    are consistent with that reported by BC92 and with recent observations of *Melling et al.* [2015]

132    and *Haas and Howell* [2015]. The standard deviations are nearly uniform (at ~0.2 m) across all

133    sites, giving a relatively low coefficient of variation (CV; a measure of relative dispersion

134    defined as the ratio of the standard deviation to the mean) of ~0.1. The thickest ice is found in

135    Eureka with a 1957-2014 mean of 2.27 m, which is likely due to climatologically lower air

136    temperatures in the fall and winter (Table 3).

137         Snow depth also appears to grow linearly through the season, peaking in May but unlike

138    ice thickness the monthly variability is high (CV ~0.4) (Figure 3).  Mean October to May snow

139   depths at Resolute, Eureka and Alert range from ~18-23 cm compared to only ~8 cm at

140   Cambridge Bay (Table 3). The rapid buildup of the snow cover due to storms in the fall and early

141   winter that is evident over the Arctic Ocean multi-year ice cover [*Warren et al.,* 1999; *Webster et*

142   *al.,* 2014], is not seen in these snow depth records within the CAA. The linear behavior in snow

143   depth is likely maintained by continuous wind-driven redistribution and densification throughout

144   the ice growth season [BC92; *Woo and Heron*, 1989].

145

146   **3.2. Trends**

147        The time series of maximum ice thickness at Cambridge Bay, Resolute, Eureka and Alert

148   are illustrated in Figure 4 and summarized in Table 1. Statistically significant (95% or greater

149   confidence level) negative maximum ice thickness trends are present at Cambridge Bay (-

150   $4.31\pm1.4$ cm decade$^{-1}$), Eureka (-4.65$\pm$1.7 cm decade$^{-1}$) and Alert (-4.44$\pm$1.6 cm decade$^{-1}$) (Table

151   1). A slight negative trend is present at Resolute but not statistically significant at the 95%

152   confidence level (Table 1). Over the 50+ year record, the ice thinned by ~0.24-0.26 m at

153   Cambridge Bay, Eureka and Alert with essentially negligible change at Resolute. These trends in

154   the CAA are similar to trends on the Siberian coast (-3.3 cm decade$^{-1}$) [*Polyakov et al.,* 2010] but

155   lower in magnitude compared to the Barents Sea (-11 cm decade$^{-1}$) [*Gerland et al.,* 2008].

156        For the shorter record (late 1950s–1989, ~30 years) investigated by BC92 there was a

157   negative trend at Alert (-7.1 cm decade$^{-1}$), no evidence of a trend at Eureka, and a positive trend

158   at Resolute (10 cm decade$^{-1}$) but only the positive trend at Resolute was statistically significant at

159   the 95% or greater confidence level. Our results from the present 50+ year record suggest that

160   the negative trend at Alert is robust and the trend at Eureka is now negative and significant. The

161   trend at Resolute is now slightly negative however it is not statistically significant.

162     Typically, ice thickness reaches its maximum in late May with trends toward earlier dates

163     of maximum ice thickness present at all sites (significant at Resolute, Eureka and Alert; Table 3).

164     The significant trends are between -2.0±0.1 days decade$^{-1}$ at Eureka to -6.2±1.5 days decade$^{-1}$ at

165     Resolute. At Resolute, the date of maximum ice thickness is now on average more than a month

166     earlier than the early 1960's although this is not reflected in the trend in ice thickness. Freeze

167     onset at these sites is also increasing at ~3-6 days decade$^{-1}$ [*Howell et al.,* 2009] and

168     demonstrates a shortened growth season at Resolute, Eureka and Alert. Together, the trends of

169     ice thickness and their recorded dates suggest a systematic thinning of landfast ice at Cambridge

170     Bay, Eureka and Alert.

171

172     **3.3. Ice thickness linkages with snow depth and temperature**

173     The variability of landfast thickness at these Arctic sites was previously found to be

174     largely driven by interannual variations in snow depth and air temperature [BC92; *Flato and*

175     *Brown*, 1996]. With the 50+ year record at the four sites, we can examine the corresponding

176     linkages to snow depth and temperature.

177     For snow depth, the only trend that is statistically significant at the 95% confidence is

178     Cambridge Bay at -0.8±0.4 cm decade$^{-1}$ (Table 3). In contrast, BC92 found a significant positive

179     trend at Alert (4 cm decade$^{-1}$), a trend of low significance in Eureka, and a negative and

180     significant trend at Resolute (-3.3 cm decade$^{-1}$). Looking at the detrended correlations (r)

181     between snow depth and ice thickness reveals the strongest correlation at Resolute (r=-0.71)

182     followed by Eureka (r=-0.66), Alert (r=-0.47) and Cambridge Bay (r=-0.31). Figure 6 provides

183     evidence from extreme years of the role of deeper snow inhibiting ice growth compared to

184     thinner snow, but the positive trends in snow thickness are not significant at Resolute, Eureka

185 and Alert. This may in part be due to the single pointwise snow depth and ice thickness
186 measurements made at each point in time, which fail to capture spatial heterogeneity in the snow
187 depth/ice thickness relationship.

188     With respect to observed temperature, we find significant warming trends in the spring
189 and fall at all sites over the 50+ year record (Table 3; Figure 7). Significant warming is also
190 present at all sites in the summer except Resolute and at all sites during the winter except Eureka
191 (Table 3). Warming is highest during the fall, at ~0.6°C decade$^{-1}$ at all sites (Table 3). The
192 detrended correlation between temperature (winter, spring, summer and autumn) and maximum
193 ice thickness is weak at all sites. For example, the strongest detrended correlation between
194 maximum ice thickness and temperature (winter and spring) is found at Cambridge Bay during
195 the winter and spring but is only ~0.4.

196     Also of interest is that the observed temperature trends over this period differ
197 considerably from the earlier period investigated in BC92, in which they reported cooling at all
198 the sites, with a significant cooling trend at Eureka. It was noted that the general cooling over
199 their record coincided with the 1946-1986 cooling trend over much of the eastern Arctic and
200 northwest Atlantic reported by *Jones et al.* [1987]. This cooling trend halted during the 1980s
201 and the warming, seen in the current and longer record, has resumed [*Jones et al.,* 1999]. Arctic
202 land areas have experienced an overall warming of about ~2°C since the mid-1960s, with area-
203 wide positive temperature anomalies that show systematic changes since the end of the 20th
204 century, which continued through 2014 [J*effries and Richter-Menge*, 2015]. Recently, warming
205 in Canadian Arctic regions was found to be greater than the pan-Arctic trend by up to 0.2°C
206 decade$^{-1}$ [*Tivy et al.,* 2011].

207

**4. Results and Discussion: Models**

**4.1. Climatology**

In order to compare seasonal cycles and trends in landfast ice thickness and snow depth between models and observations, we limit our comparison to models with a reasonable representation of the CAA, i.e. those with an open Parry Channel (i.e. bcc-csm-1-1, bcc-csm-1-1m, CNRM-CM5, ACCESS1-0, ACCESS1-3, FIO-ESM, EC-EARTH, inmcm4, MIROC5, MPI-ESM-LR, MPI-ESM-MR, MRI-CGCM3, CCSM4, NorESM1-M, NorESM1-ME, GFDL-CM3, GFDL-ESM2G, GFL-ESM2M, CESM1-BCG, CESM1-CAM5, CESM-WACCM). In these models, sufficient spatial resolution allows us to find sample points that are almost collocated to *in situ* observation locations. The sample points were determined by finding the closest ocean grid point where the sea ice is packed for a good portion of the year, but not all year. Grid points with this characteristic therefore share the most important feature of the landfast ice at our observations locations: it is not perennial. Mathematically, we sought sample points where the sea ice concentration is on average above 85% for more than one month but less than 11 months over the 1955-2014 period. The Eureka site is however particularly challenging for models because it lies deep in a very narrow channel, which is only resolved by the MPI-ESM-MR in the CMIP5. As a result, for most models, the sample point for Eureka is located on the western shore of Ellesmere Island. This is a consequence of using samples as some models either do not resolve some of the channels in the CAA or have too perennial packed ice cover (e.g. CESM1-CAM5), then the sample points are further from the observational site than would be desired. We chose to use sample points in our comparison to observations instead of using regional averages for two main reasons. The first reason is that using regional averages would have lumped together different ice dynamics regimes that should not necessarily be expected to compare well

231    to point observations on landfast ice. The second reason is that we are of the opinion that the

232    resolution in many of these models is sufficiently high to warrant such a direct comparison and

233    provides a better benchmark than regional averages for landfast ice modelling in the CAA.

234          The seasonal cycle (1955-2014) of median ice thickness from CMIP5 (black), ORA-IP

235    models CGLORS, ORAP5.0 and GLORYS2V3 (blue), ECCO-v4 (green) and UR025.4 (red) is

236    shown in Figure 8. ORA-IP models have been split into three groups based, respectively, on their

237    high, medium and low ice thicknesses at Alert. Ice thickness from CMIP5 is comparable to

238    observations (Figure 2) at Cambridge Bay and Resolute with maximum ice thickness reaching

239    200 cm. The ORA-IP models are less consistent. ECCO-v4 tends to have thicker sea ice than

240    observations at Cambridge Bay, Resolute and Eureka but thinner at Alert. CGLORS, ORAP5.0,

241    and GLORYS2V3, on the other hand, are comparable to observations at Cambridge Bay,

242    Resolute and Eureka but have extremely thick and perennial ice close to Alert.

243          The seasonal cycle (1955-2014) of median snow depth from CMIP5 is shown in Figure

244    9. CMIP5 models indicate a linear increase similar to observations reaching a maximum of ~20

245    cm in April or May. This is lower than the observed maximum at Resolute, Eureka and Alert but

246    is about twice as much as at Cambridge Bay. While the snow depth reaches zero during the

247    summer at Eureka and Alert in models, the sea ice thickness does not (Figure 8), unlike in

248    observations. This likely reflects the fact that the grid cell thickness in sea ice models with

249    thickness classes a represents the average thickness over these classes. In August the thinner ice

250    classes might have melted but thicker ice classes can still be found, resulting in a substantial

251    average ice thickness over the grid cell. The seasonal cycle over packed ice in these models thus

252    gives a reasonable representation of the seasonal cycle over landfast ice in the CAA, especially

253    in the southern region of the CAA. Overall, this comparison shows how recent improvements in

254    sea ice model resolution allows comparisons with observations that required dynamical

255    downscaling techniques in the previous generation of sea ice models [i.e. *Dumas et al. 2005; Sou*

256    *and Flato, 2013*].

257        Despite relatively high spatial resolution, PIOMAS does not resolve seasonal ice

258    thickness along the coasts and within the very narrow channels within the CAA (not shown). As

259    a result, Cambridge Bay and Resolute Bay sites represent the only long-term monitoring sites

260    within the CAA suitable for comparison since PIOMAS. The monthly time series of PIOMAS

261    ice and snow thickness estimates at Cambridge Bay and Resolute is shown in Figure 10. The

262    seasonal cycle of ice growth at Cambridge Bay and Resolute is representative compared to

263    observations (Figure 2) but PIOMAS estimates retain more ice in August and September,

264    particularly at Resolute. Ice growth reaches a maximum in April at Cambridge and in May at

265    Resolute which is 1-month earlier compared to observations. Snow depth follows a linear

266    increase similar to observations (Figure 3) with good agreement at Cambridge Bay but

267    considerably underestimates snow depth at Resolute (Figure 10). *Schweiger et al.* [2011]

268    performed a detailed comparison of PIOMAS ice thickness values against *in situ* and Ice, Cloud,

269    and land Elevation Satellite (ICESat) ice thickness observations and found strong correlations.

270    They determined a root mean square error (RMSE) of ~0.76 m and noted that PIOMAS

271    generally overestimates thinner ice and underestimates thicker ice. At both sites within the CAA,

272    PIOMAS ice thickness data is in reasonably good agreement with *in situ* observations with

273    RMSE's of 0.29 cm at Cambridge Bay and 0.68 cm at Resolute (Figure 11). The systematic

274    overestimate of thinner ice reported by *Schweiger et al.* [2011] is more apparent at Resolute than

275    Cambridge Bay (Figure 11).  The  higher latitude regions of the CAA where there is an intricate

276  mix of seasonal first-year ice and multi-year ice is a problem for PIOMAS and thus contributes

277  to the larger discrepancy at Resolute compared to Cambridge Bay.

278

279  **4.2. Trends**

280  The spatial distribution of maximum sea ice thickness trends from ORA-IP and CMIP5 is

281  illustrated in Figures 12. The CMIP5 model-mean exhibit a fairly uniform trend pattern,

282  consistent with the different in situ observations (Figure 4) but with overestimated negative

283  thickness trends. Although, for individual models this pattern is far from uniform, the general

284  pattern and magnitude of thickness trends tend to be roughly in accordance with temperature

285  trends (not shown). A similar behavior is observed in the ORA-IP models, with the notable

286  exception of CGLORS, where positive thickness trends are found almost everywhere (Figure

287  12a). This is robust and it appears that the model is not completely equilibrated in the CAA and

288  exhibit large month-to-month adjustments. Model ORAP5.0 also is not completely equilibrated

289  in the region for years 1979-1984. During those years, it exhibits large inter annual changes in

290  thickness. For this reason, we are only considering years 1985-2013 for this model.

291  For PIOMAS, the North-South overestimated trend is also present (not shown) as with

292  CMIP5 and ORA-IP. Looking specifically at trends computed from 1979-2014 near the observed

293  sites indicates that the mean maximum ice thickness linear trend from at Cambridge Bay is -

294  $13.4+3.4$ cm decade$^{-1}$ which is almost double the observational trend of $6.2\pm2.4$ cm decade$^{-1}$. At

295  Resolute, the PIOMAS linear trend is $24.0\pm4.1$ cm decade$^{-1}$ which is considerably stronger than

296  the observational trend of $-4.9\pm3.51$ cm decade$^{-1}$.

297

298  **4.3. Ice thickness linkages with snow depth and temperature**

299     Even though ORA-IP models have unrealistically large thickness trends, the pattern of

300     inter annual correlation (detrended) between winter temperatures and thicknesses is roughly

301     consistent across models (Figure 13). Some ORA-IP models also experience positive correlations

302     (e.g. CGLORS, ORAP5.0, GLORYS2V3 and UR025.4) that are mostly located north of the

303     CAA or within the CAA in regions where multi-year ice is known to be present.  It is possible

304     that warmer temperatures are associated with an increased flux of thicker multi-year ice into the

305     CAA which is known to occur [e.g. *Howell et al.,* 2013] but the driving processes responsible for

306     these positive correlations require more investigation. In CMIP5 models, no model exhibits

307     positive correlations with temperature that resemble ORA-IP models over the CAA. Although

308     the time series for the ORA-IP models is short and the positive correlations are only statistically

309     significant at a few grid points in CGLORS and UR025.4, this behavior is sufficiently

310     problematic to recommend that care should be taken when using these ORA-IP models to study

311     the interannual variability in the Canadian Arctic.

312     In the CMIP5 models, significant winter snow depth trends are more strongly negative in

313     the North than in the South (Figure 14). This is in disagreement with point observations

314     presented in the previous sections that showed no significant trends snow depth trends at Alert

315     but negative and significant trends at Cambridge Bay. Although only based on limited point *in*

316     *situ* observations, this suggests that over the last decades changes in winter precipitation at Alert

317     must have compensated the increased melting driven by increasing temperatures, a compensation

318     that is clearly not captured in CMIP5 models..

319

320     **5. Conclusions**

321       Over the 50+ year in situ observational record, statistically significant negative trends in

322    maximum (end-of-winter) ice thickness are present at Cambridge Bay, Eureka and Alert.

323    Significant negative trends in the day of maximum ice thickness are also present at Resolute,

324    Eureka and Alert. Together, these trends suggest thinning of landfast ice in the CAA, where little

325    evidence was found in the shorter record analyzed in an earlier study (BC92). The inter-annual

326    variability of air temperature is only weakly correlated to maximum ice thickness (i.e. maximum

327    correlation is ~0.4).  Snow thickness plays the dominant role in controlling maximum ice

328    thickness variability given the high correlations at Resolute and Eureka and reasonably high

329    correlations at Alert and Cambridge Bay.

330       Comparison of CMIP5, ORA-IP and PIOMAS simulations with observations indicate a

331    reasonable representation of the landfast ice thickness monthly climatology within the CAA.

332    This is particularly apparent when seasonal first-year ice dominates the icescape (i.e. Cambridge

333    Bay). Despite improvements in spatial resolution, mixed ice types (i.e. seasonal and multi-year)

334    present at the sub-grid cell resolution are likely problems for model estimates within the CAA.

335    The overall thickness of ice within the CAA in the current generation of models is too high. As a

336    result, trends are unrealistic and far exceed observations (by upwards of -50 cm decade$^{-1}$) in part

337    because the initial ice thickness is too large. The problem is particularly acute in the ORA-IP

338    models where large and unrealistic inter annual changes in thickness suggest that the models are

339    not fully equilibrated.

340       While the impact of the snow cover on ice thickness is well known, the significant

341    correlations at Resolute, Eureka and Alert suggest that the higher sensitivity to changes in snow

342    depth could potentially mask the warming signal on both fast and offshore ice. Thus, even in this

343    limited data set, we can see the dominant role played by snow depth in determining the

344 interannual variability of the maximum landfast ice thickness. This again highlights that the

345 primary factor is the amount and timing of snow accumulation, not air temperature. However, it

346 is worth noting that few of the current generation models show coherent relationships between

347 ice thickness, snow depth and temperature over the longer term record.

348

349 **Appendix**

350 The Monte-Carlo simulation used to combine trends and Pearson correlations is applied

351 at each grid point independently. Models that have a land mask at a grid point are discarded

352 before starting the procedure.

353 A noise model is created to ensure that internal variability is comparable for models with

354 different ensemble sizes, following Swart et al. [2014] and Laliberté et al. [2016]. To generate

355 the noise model, we discard models that have fewer than two realizations. From the remaining

356 models, we pick one and then one of its realizations. We then record to the noise model the

357 difference of this realization's trend from the mean trend of the model's realizations, multiplied

358 by $(n/(n-1))^{1/2}$, with n being the number of realizations, to account for the fact that some models

359 have such a small number of realizations that it cannot completely account for the internal

360 variability. We repeat this procedure 1000 times and compute the variance $\sigma n$ of the noise

361 model.

362 We then pick a model from which we select 1000 realizations, allowing repetitions. For

363 each one of these realizations, we select a random value from its trend t-distribution. If the inter-

364 realization trend variance $\sigma_m$ is smaller than the variance of the noise model $\sigma_n$, we then draw a

365 random value from the noise model, multiply it by $(1-\sigma_m/\sigma_n)^{1/2}$ and add it to the random value

366 from the trend t-distribution.

367    We repeat this procedure with the remaining models. We then average the 1000 values

368    across models, creating a distribution for the multi-model mean trend with 1000 values. The

369    mean of this distribution gives our multi-model mean and its two-sided p-value is given by twice

370    its survival function or cumulative distribution function at 0, whichever is smallest.

371    The Pearson correlations are analyzed in the same way except that a Fisher transform

372    (obtained by the hyperbolic arctangent of the correlation) is applied first and random values are

373    drawn from a normal distribution (instead of the t-distribution) with variance $1/(T-3)$, with T the

374    number of years used for the correlation. The multi-model mean Pearson correlation is then

375    given by the inverse Fisher transform (obtained by the hyperbolic tangent of the mean) of the

376    distribution mean.

377

378    **Authors Contributions**

379    S.E.L.H, F.L and R.K designed the study, performed the analysis and wrote the manuscript with

380    input from C.D. and J.K.

381

382    **Acknowledgements**

383    The authors with to thank all the individuals responsible for collecting landfast ice and snow

384    thickness measurements in the Canadian Arctic over the past 50+ years.

385
386
387    **References**

388
389    Alt, B., K. Wilson, and T. Carrieres (2006), A case study of old ice import and export through
390    Peary and Sverdrup channels in the Canadian Arctic Archipelago: 1998-2004, *Ann. Glaciol.*, 44,
391    329–338, doi:10.3189/172756406781811321.
392
393    M.A. Balmaseda , F. Hernandez , A. Storto , M.D. Palmer , O. Alves , L. Shi , G.C. Smith , T.
394    Toyoda , M. Valdivieso , B. Barnier , D. Behringer , T. Boyer , Y-S. Chang , G.A. Chepurin , N.

395    Ferry , G. Forget , Y. Fujii , S. Good , S. Guinehut , K. Haines , Y. Ishikawa , S. Keeley , A.
396    Köhl , T. Lee , M.J. Martin , S. Masina , S. Masuda , B. Meyssignac , K. Mogensen , L. Parent ,
397    K.A. Peterson , Y.M. Tang , Y. Yin , G. Vernieres , X. Wang , J. Waters , R. Wedd , O. Wang ,
398    Y. Xue , M. Chevallier , J-F. Lemieux , F. Dupont , T. Kuragano , M. Kamachi , T. Awaji , A.
399    Caltabiano , K. Wilmer-Becker , F. Gaillard, The Ocean Reanalyses Intercomparison Project
400    (ORA-IP), *Journal of Operational Oceanography*, Vol. 8, Iss. sup1, 2015,
401    DOI:10.1080/1755876X.2015.1022329

403    Brown, R., and P. Cote (1992), Interannual variability of landfast ice thickness in the Canadian
404    high arctic, 1950–89. *Arctic*, 45, 273–284.

406    Bromwich, D. H., A. B. Wilson, L. Bai, G. W. K. Moore, and P. Bauer, 2015: A comparison of
407    the regional Arctic System Reanalysis and the global ERA-Interim Reanalysis for the Arctic. *Q.*
408    *J. R. Meteorol. Soc.*, doi: 10.1002/qj.2527

410    Dee DP, co-authors (2011), The ERA-Interim reanalysis: configuration and performance of the
411    data assimilation system. *Q J R Meteorol Soc*. 137: 553–597, doi:10.1002/qj.828.

413    Dumas, J. A., G. M. Flato, and R. D. Brown (2006), Future projections of landfast ice thickness
414    and duration in the Canadian Arctic. *J. Climate*, 19, 5175–5189.

416    Druckenmiller, M. L., H. Eicken, M. A. Johnson, D. J. Pringle, and C. C. Williams (2009),
417    Toward an integrated coastal sea-ice observatory: System components and a case study at
418    Barrow, Alaska. *Cold Reg.Sci.Tech.*, 56, 61-72.

420    Flato, G. M., and R. D. Brown (1996),Variability and climate sensitivity of landfast Arctic sea
421    ice. *J. Geophys. Res*., 101 (C10), 25 767–25 777.

423    Forget, G., Campin, J.-M., Heimbach, P., Hill, C. N., Ponte, R. M., and Wunsch, C. (2015),
424    ECCO version 4: an integrated framework for non-linear inverse modeling and global ocean
425    state estimation, *Geosci. Model Dev*., 8, 3071-3104, doi:10.5194/gmd-8-3071-2015/

427    Gerland, S., A. H. H. Renner, F. Godtliebsen, D. Divine, and T. B. Loyning (2008), Decrease of
428    sea ice thickness at Hopen, Barents Sea, during 1966-2007. *Geophys. Res. Lett*., 35, L06501.

430    Gough, W., A.S. Gagnon an H.P Lau (2004), Interannual variability of Hudson Bay Ice
431    Thickness, *Polar Geography*, 28(3), 222-238.

433    Haines K, M. Valdivieso, H. Zuo, and V.N. Stepanov (2012), Transports and budgets in a 1/4 °
434    global ocean reanalysis 1989–2010. *Ocean Sci.* 8(3): 333–344, doi:10.5194/os-8-333-
435    2012.002/qj.2063.

437    Haas, C., and S. E. L. Howell (2015), Ice thickness in the Northwest Passage, *Geophys. Res.*
438    *Lett.*, 42, doi:10.1002/2015GL065704

440 Howell, S. E. L., C. R. Duguay, and T. Markus (2009), Sea ice conditions and melt season
441 duration variability within the Canadian Arctic Archipelago: 1979–2008, Geophys. Res. Lett.,
442 36, L10502, doi:10.1029/2009GL037681.

443 Howell, S. E. L., T. Wohlleben, M. Dabboor, C. Derksen, A. Komarov, and L. Pizzolato (2013),
444 Recent changes in the exchange of sea ice between the Arctic Ocean and the Canadian Arctic
445 Archipelago, *J. Geophys. Res. Oceans*, 118, 3595–3607, doi:10.1002/jgrc.20265.
446 Jeffers, S., T. Agnew, B. Alt, R. De Abreu, and S. McCourt (2001), Investigating the anomalous
447 sea ice conditions in the Canadian High Arctic (Queen Elizabeth Islands) during the summer of
448 1998, *Ann. Glaciol.*, 33, 507– 612.
449
450 Jeffries, M. O. and J. Richter-Menge, Eds. (2015), The Arctic [in State of the Climate in 2014],
451 *Bull. Amer. Meteor. Soc.*, 96, ES1–ES32.
452 doi: http://dx.doi.org/10.1175/2015BAMSStateoftheClimate.1
453
454 Jones, P.D., T.M.L. Wigley, C.K. Folland and D.E. Parker (1987), Spatial patterns in recent
455 worldwide temperature trends. *Climate Monitor*, 16(5): 175-185.
456
457 Jones, P.D., M. New, D.E. Parker, S. Martin, and I.G. Rigor (1999), Surface air temperature and
458 its changes over the past 150 years, *Rev. Geophys*, 37(2),173–200.
459
460 Kwok, R., and D. A. Rothrock (2009), Decline in Arctic sea ice thickness from submarine and
461 ICESat records: 1958 – 2008, *Geophys. Res. Lett.*, 36, L15501, doi:10.1029/2009GL039035.
462
463 Laliberté, F., S. E. L. Howell, and P. J. Kushner (2016), Regional variability of a projected sea
464 ice-free Arctic during the summer months, *Geophys. Res. Lett.*, 43, 256–263,
465 doi:10.1002/2015GL066855.
466
467 Laxon S. W., K. A. Giles, A. L. Ridout, D. J. Wingham, R. Willatt, R. Cullen, R. Kwok, A.
468 Schweiger, J. Zhang, C. Haas, S. Hendricks, R. Krishfield, N. Kurtz, S. Farrell and M. Davidson
469 (2013), CryoSat-2 estimates of Arctic sea ice thickness and volume, *Geophys. Res. Lett.*, 40,
470 732–737, doi:10.1002/grl.50193.
471
472 Masina, S. et al. (2015), An ensemble of eddy-permitting global ocean reanalyses from the
473 MyOcean project. *Clim. Dynam*. 1–29, doi:10.1007/s00382-015-2728-5
474
475 Mahoney, A., H. Eicken, and L. Shapiro (2007), How fast is landfast sea ice? A study of the
476 attachment and detachment of nearshore ice at Barrow, Alaska. *Cold Reg.Sci.Tech.*, 47, 233-255.
477
478 Mahoney, A. R., H. Eicken, A. G. Gaylord, and R. Gens (2014), Landfast sea ice extent in the
479 Chukchi and Beaufort seas: The annual cycle and decadal variability, Cold Reg. Sci. Technol. ,
480 103, 41–56, doi:10.1016/j.coldregions.2014.03.003.

481 Melling, H. (2002), Sea ice of the northern Canadian Arctic Archipelago, *J. Geophys. Res.*,
482 107(C11), 3181, doi:10.1029/2001JC001102.

483

484      Melling, H., C. Haas, and E. Brossier (2015), Invisible polynyas: Modulation of fast ice
485      thickness by ocean heat flux on the Canadian polar shelf, *J. Geophys. Res. Oceans*, 120, 777–
486      795, doi:10.1002/2014JC010404.

487      Ólason, E. Ö. (2012), Dynamical modeling of Kara Sea land-fast ice, PhD thesis, Univ. of
488      Hamburg, Hamburg, Germany.
489
490      Polyakov, I. V., et al. (2010), Arctic Ocean Warming Contributes to Reduced Polar Ice Cap.
491      *Journal of Physical Oceanography*, 40, 2743-2756
492
493      Schweiger, A., R. Lindsay, J. Zhang, M. Steele, H. Stern, and R. Kwok (2011), Uncertainty in
494      modeled Arctic sea ice volume, *J. Geophys. Res*., 116, C00D06, doi:10.1029/2011JC007084.
495
496      Serson, H.V. (1972), Investigations of a plug of multiyear old sea icein the mouth of Nansen
497      Sound. Ottawa, Ont., Department of National Defence, Canada. Defence Research Establishment
498      Ottawa. (DREO Tech. Note 72-6.)
499
500      Serson, H.V. (1974), Sverdrup Channel. Ottawa, Ont., Department of National Defence, Canada.
501      Defence Research Establishment Ottawa. (DREO Tech. Note 74-10.)
502
503      Sou, T., and G. Flato (2009), Sea ice in the Canadian Arctic Archipelago: Modeling the past
504      (1950-2004) and the future (2041-60), J. Clim., 22, 2181–2198, doi:10.1175/2008JCLI2335.1
505      Stroeve, J. C., M. C. Serreze, M. M. Holland, J. E. Kay, J. Malanik, and A. P. Barrett (2011),
506      The Arctic's rapidly shrinking sea ice cover: A research synthesis, *Clim. Change*, 110(3-4),
507      1005–1027.
508
509      Storto A, S. Dobricic S, S. Masina and D. Di Pietro (2011), Assimilating along-track altimetric
510      observations through local hydrostatic adjustments in a global ocean reanalysis system. *Mon*
511      *Wea Rev*. 139: 738–754.
512
513      Stroeve, J. C., M. C. Serreze, M. M. Holland, J. E. Kay, J. Maslanik, and A. P. Barrett (2012),
514      The Arctic's rapidly shrinking sea ice cover: A research synthesis, *Clim. Change*, 110(3–4),
515      1005–1027

516      Swart, N. C., J. C. Fyfe, E. Hawkins, J. E. Kay, and A. Jahn (2015), Influence of internal
517      variability on Arctic sea-ice trends, *Nat. Clim. Change*, 5, 86–89, doi:10.1038/nclimate2483.
518
519      Taylor, K. E., R. J. Stouffer, and G. A. Meehl (2012), An overview of CMIP5 and the
520      experiment design, *Bull. Am. Meteorol. Soc*., 93, 485–498, doi:10.1175/BAMS-D-11-00094.1.
521
522      Tivy, A., S. E. L. Howell, B. Alt, S. McCourt, R. Chagnon, G. Crocker, T. Carrieres, and J. J.
523      Yackel (2011), Trends and variability in summer sea ice cover in the Canadian Arctic based on
524      the Canadian Ice Service Digital Archive, 1960–2008 and 1968–2008, *J. Geophys. Res*., 116,
525      C03007, doi:10.1029/2009JC005855.
526

527  Vincent, L., X. Wang, E. Milewska, Hui Wan, F. Yang, and V. Swail (2012), A second
528  generation of homogenized Canadian monthly surface air temperature for climate trend analysis.
529  *Journal of Geophysical Research*, D18110, doi:10.1029/2012JD017859
530
531  Warren, S. G., I. G. Rigor, N. Untersteiner, V. F. Radionov, N. N. Bryazgin, Y. I. Aleksandrov,
532  and R. Colony (1999), Snow depth on Arctic sea ice*, J. Clim*., 12, 1814– 1829.
533
534  Wilks, D. S. (2006). On "field significance" and the false discovery rate. *J. Appl. Meteor.*
535  *Climatol*., 45, 1181–1189. doi: http://dx.doi.org/10.1175/JAM2404.1
536  Woo, M-K., and R. Heron (1989), Freeze-up and break-up of ice cover on small arctic lakes. In:
537  Mackay, W.C., ed. Northern lakes and rivers. Edmonton: Boreal Institute for Northern Studies,
538  56-62.
539
540  Woo, M-K., R. Heron, P. Marsh, and P. Steer, (1983), Comparison of weather station snowfall
541  with winter snow accumulation in High Arctic basins, *Atmos.-Ocean*, 21(3):312-325.
542
543  World Meteorological Organization, (1970), WMO sea-ice nomenclature. Terminology, codes
544  and illustrated glossary. WMO/OMM.BMO No. 259, 145 pp, Geneva Secretariat of the World
545  Meteorological Organization
546
547  Yu, Y, H. Stern, C. Fowler, F. Fetterer, and J. Maslanik (2014), Interannual Variability of Arctic
548  Landfast Ice between 1976 and 2007. *J. Climate*, **27**, 227–243.
549  doi: http://dx.doi.org/10.1175/JCLI-D-13-00178.1
550
551  Zhang, J.L. and D.A. Rothrock, (2003), Modeling global sea ice with a thickness and enthalpy
552  distribution model in generalized curvilinear coordinates, *Mon. Weather Rev*., 131, 845-861.
553  Zuo, H., M.A. Balmaseda, and K. Mogensen (2015), The new eddy-permitting ORAP5 ocean
554  reanalysis: description, evaluation and uncertainties in climate signals. *Clim. Dynam*. 1–21.
555  doi:10.1007/s00382-015-2675-1.
556
557
558
559
560
561
562
563
564
565
566
567
568
569
570
571
572

573 Table 1. CMIP5 models used in this study, the number of realizations with ice data and the
574 number of realizations with sea ice transport data

| | w/ ice | | w/ ice |
|---|---|---|---|
| bcc-csm1-1 | 1 | MIROC-ESM-CHEM | 1 |
| bcc-csm1-1-m | 1 | MIROC5 | 3 |
| BNU-ESM | 1 | HadGEM2-CC | 1 |
| CanESM2 | 5 | HadGEM2-ES | 4 |
| CMCC-CESM | 1 | MPI-ESM-LR | 3 |
| CMCC-CM | 1 | MPI-ESM-MR | 1 |
| CMCC-CMS | 1 | MRI-CGCM3 | 1 |
| CNRM-CM5 | 5 | CCSM4 | 6 |
| ACCESS1.0 | 1 | NorESM1-M | 1 |
| ACCESS1.3 | 1 | NorESM1-ME | 1 |
| CSIRO-Mk3.6.0 | 10 | GFDL-CM3 | 1 |
| FIO-ESM | 1 | GFDL-ESM2G | 1 |
| EC-EARTH | 6 | GFDL-ESM2M | 1 |
| inmcm4 | 1 | CESM1(BGC) | 1 |
| FGOALS-g2 | 1 | CESM1(CAM5) | 3 |
| MIROC-ESM | 1 | CESM1(WACCM) | 3 |

575
576
577
578
579
580
581
582
583
584
585
586
587
588
589
590
591
592
593

594    Table 2. Summary of ORA-IP models characteristics

| Model Name | CGLORS | ECCO-v4 | GLORYS2V3 | ORAP5.0 | UR025.4 | PIOMAS |
|---|---|---|---|---|---|---|
| Institute | CMCC | JPL-NASA-MIT-AER | Mercator Océan | ECMWF | University of Reading | APL/PSC |
| Resolution | ORCA0.25° | ~40km in the Arctic | ORCA0.25° | ORCA0.25° | ORCA0.25° | ~22km in the Arctic |
| Ocean Model | NEMO 3.2.1 | MITgcm | NEMO 3.1 | NEMO3.4 | NEMO 3.2 | POP |
| Sea ice Model | LIM2 | MITgcm | LIM2 (with EVP rheology) | LIM2 | LIM2 | TED |
| Time period considered | 1982-2012 | 1991-2011 | 1993-2013 | 1985-2013 | 1993-2010 | 1958-2015 |
| Atmospheric forcing | ERA-Interim | ERA-Interim | ERA-Interim | ERA-Interim | ERA-Interim | NCEP/NCAR |
| Sea ice product assimilated | NSIDC NASA-Team Daily | NSIDC Bootstrap Monthly | IFREMER/CERSAT | NOAA / OSTIA combination | EUMETSAT OSI-SAF | NSIDC near-real time Daily |

595
596
597
598
599
600
601
602
603
604
605
606
607
608
609
610
611
612
613
614
615
616
617
618

619 Table 3. Observed maximum ice thickness, snow depth, and surface air temperature at four
620 landfast ice sites in the Canadian Arctic Archipelago. The bold text indicates statistical
621 significance of the linear trend at 95% or greater.

|  | Cambridge Bay | Resolute | Eureka | Alert |
|---|---|---|---|---|
| Period | 1960-2014 | 1957-2014 | 1957-2014 | 1957-2014 |
| Ice Thickness, $h_{ice}$ |  |  |  |  |
| Mean of *max* $h_{ice}$ (m) | 2.11±0.19 | 2.02±0.19 | 2.27±0.23 | 1.98±0.22 |
| Trend of *max* $h_{ice}$ (cm decade$^{-1}$) | **-4.31±1.4** | -0.5±1.6 | **-4.65±1.7** | **-4.44±1.6** |
| Day of *max* $h_{ice}$ | 24 May±17 | 25 May±21 | 26 May±12 | 27 May±16 |
| Trend of day of *max* $h_{ice}$ (days decade$^{-1}$) | -0.87±1.5 | **-6.2±1.5** | **-2.0±0.1** | **-3.0±1.2** |
|  |  |  |  |  |
| Snow depth ($h_{snow}$) |  |  |  |  |
| Mean Oct-May $h_{snow}$ (cm) | 8.4±4.2 | 22.6±10 | 17.6±5.8 | 18.4±6.2 |
| Trend of Oct-May $h_{snow}$ (cm decade$^{-1}$) | **-0.8±0.4** | -0.75±0.8 | 0.54±0.5 | 0.26±0.5 |
|  |  |  |  |  |
| Temperature |  |  |  |  |
| Winter (Dec-Feb) Mean ($^{o}$C) | -31.3±2.0 | -30.8±1.9 | -36.0±2.0 | -31.2±1.6 |
| Winter (Dec-Feb) ($^{o}$C/decade) | **0.59±0.2** | **0.35±0.1** | 0.23±0.2 | **0.38±0.1** |
| Spring (Mar-May) Mean ($^{o}$C) | -20.0±1.8 | -21.1±1.8 | -24.9±2.0 | -22.8±1.8 |
| Spring (Mar-May) ($^{o}$C/decade) | **0.47±0.1** | **0.57±0.1** | **0.44±0.1** | **0.32±0.1** |
| Summer (Jun-Aug) Mean ($^{o}$C) | 5.9±1.4 | 2.3±1.3 | 3.9±1.2 | 1.3±0.8 |
| Summer (Jun-Aug) ($^{o}$C/decade) | **0.30±0.1** | 0.17±0.2 | **0.21±0.1** | **0.1±0.1** |
| Fall (Sep-Nov) Mean ($^{o}$C) | -11.1±2.0 | -13.8±2.0 | -19.6±2.2 | -18.0±1.7 |
| Fall (Sep-Nov) ($^{o}$C/decade) | **0.60±0.2** | **0.67±0.1** | **0.68±0.2** | **0.56±0.1** |

622
623
624
625
626
627

**List of Figures**

Figure 1. Map of the central Canadian Arctic Archipelago showing the location of the landfast snow and thickness observations.

Figure 2. Seasonal cycle of observed mean ice thickness at the four sites (1960-2014).

Figure 3. Seasonal cycle of observed mean snow depth at the four sites (1960-2014).

Figure 4. Time series and trend of observed maximum ice thickness at the four sites.

Figure 5. Time series and trend of observed mean October through May snow depth at the four sites.

Figure 6. Weekly time series of ice thickness and snow depth at Eureka and Alert for (a) low snow years and (b) high snow years.

Figure 7. Time series observed mean air temperature by Environment Canada during winter (DFJ), spring, (MAM), summer (JJA) and autumn (SON) at the Cambridge Bay, Resolute, Eureka and Alert.

Figure 8. CMIP5 median sea ice thickness seasonal cycle (1955-2014) at stations (grey). Observations from 2 (black). Median of ORA-IP models CGLORS, ORAP5.0, GLORYS2V3 (blue), ECCO-v4 (green) and UR025.4 (red). Whiskers indicate the 5th and 95th percentiles.

Figure 9. Same as Figure 8 for snow depth and only for CMIP5 models (grey) and observations (black).

Figure 10. Seasonal cycle of observed mean ice thickness (left) and snow depth (right) from PIOMAS at Cambridge Bay and Resolute (1979-2014).

Figure 11. Comparison of PIOMAS ice thickness with ice thickness observations from Environment Canada's ice thickness monitoring sites at Cambridge Bay and Resolute. The data covers the period 1979-2014.

Figure 12. **a-e:** Maximum sea ice thickness trends in ORA-IP simulations. f: Same for CMIP5 MODEL-MEAN. From South to North, o's indicate Cambridge Bay (green), Resolute (blue), Eureka (white) and Alert (black) and x's indicate the corresponding measurement stations. In f, one o per model is shown." The stippling indicates p-values less than 0.05, corrected using the False Discovery Rate (FDR) method with a global pFDR-values less than 0.10 [*Wilks,* 2006]. The colorbar is linear from -10 cm dec-1 to 10 cm dec-1 and symmetric logarithmic beyond these values.

673   Figure 13. **a-e:** Pearson correlation of detrended maximum sea ice thickness in ORA-IP with
674   detrended ONDJFMAM ERA-INTERIM 2m temperature. **f:** Same but for CMIP5 MODEL-
675   MEAN. The stippling indicates p-values less than 0.05, corrected using the False Discovery Rate
676   (FDR) method with a global pFDR-values less than 0.10 [*Wilks*, 2006].
677
678   Figure 14. Same as Figure 12f but for snow depth trends (ONDFJMAM).
679
680
681
682
683
684
685
686
687
688
689
690
691
692
693
694
695
696
697
698
699
700
701
702
703
704
705
706
707
708
709
710
711
712
713
714
715
716
717
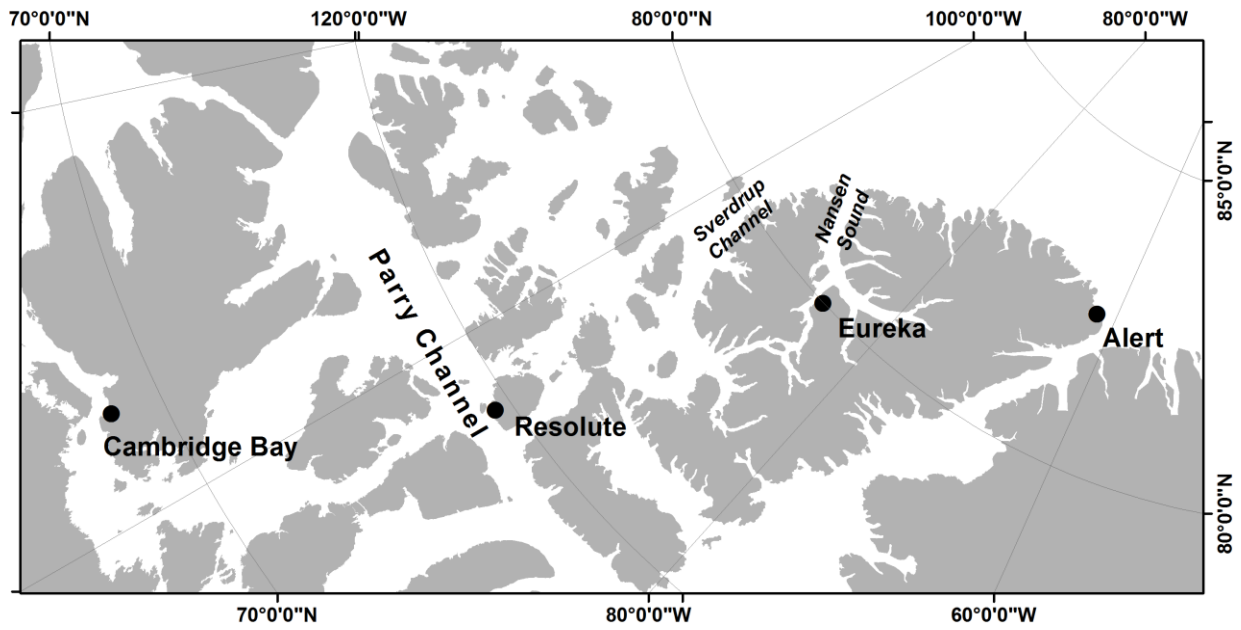
718
719 Figure 1. Map of the central Canadian Arctic Archipelago showing the location of the landfast
720 snow and thickness observations.
721
722
723
724
725
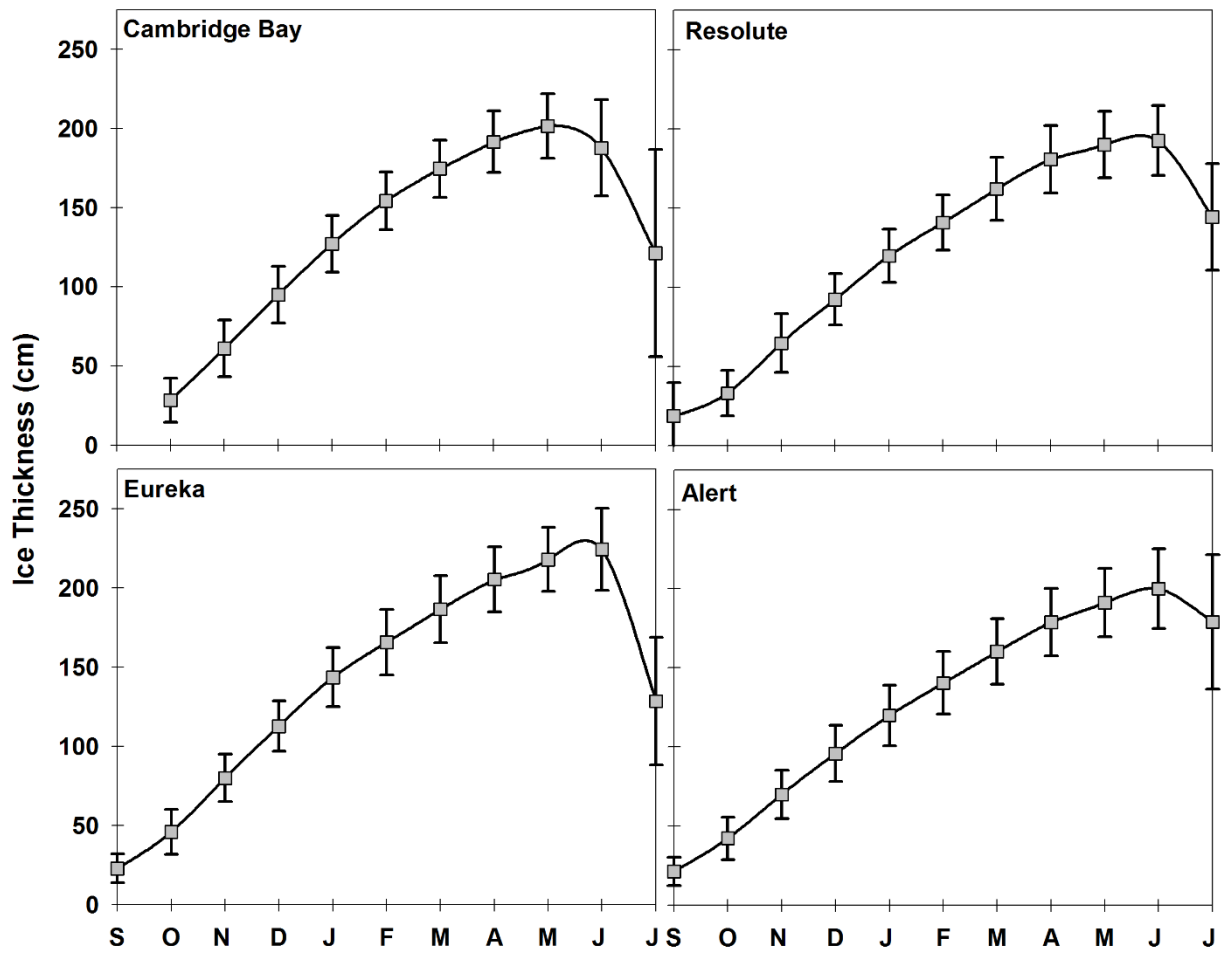
726
727 Figure 2. Seasonal cycle of observed mean ice thickness at the four sites (1960-2014).
728
729
730
731
732
733
734
735
736
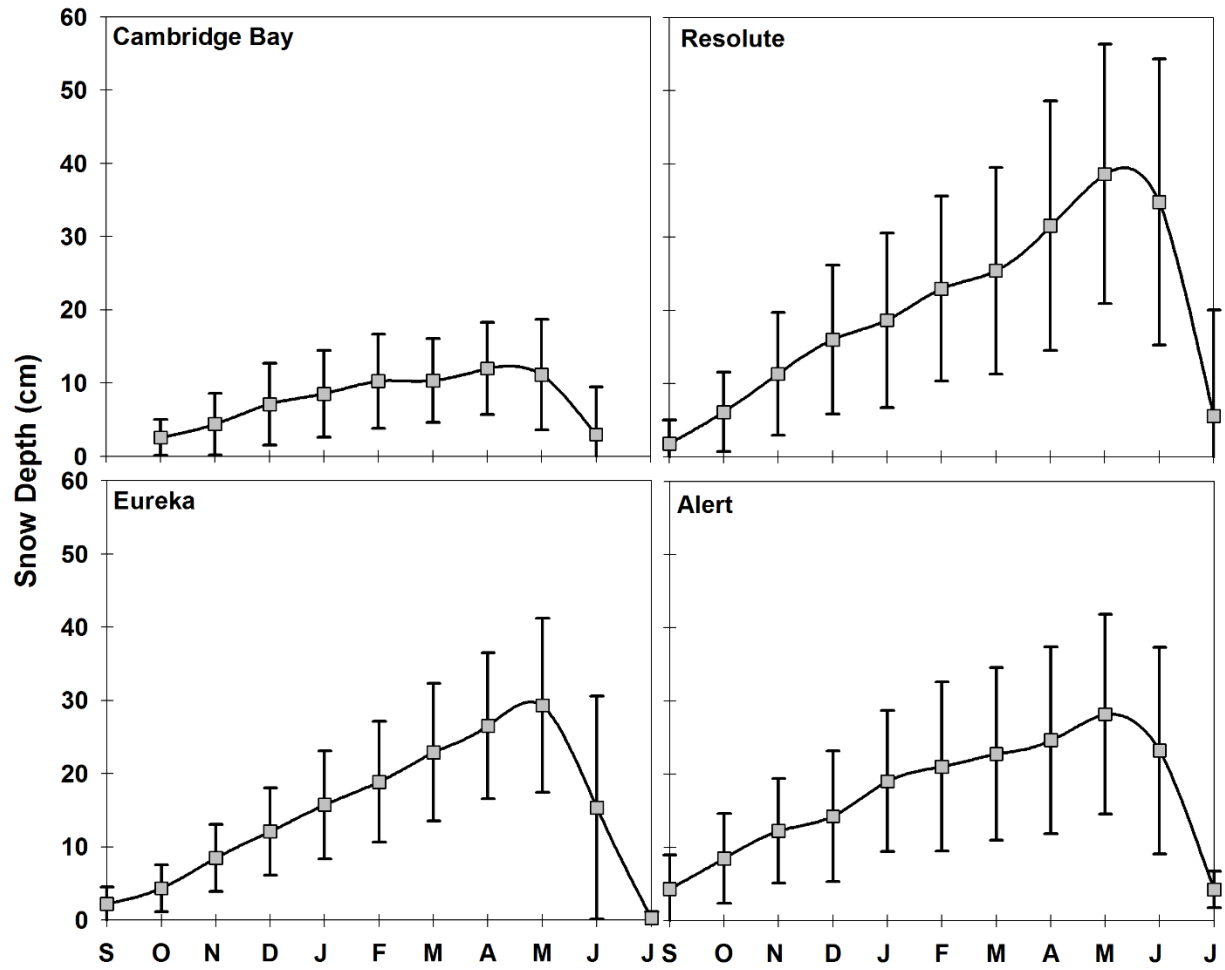
Figure 3. Seasonal cycle of observed mean snow depth at the four sites (1960-2014).
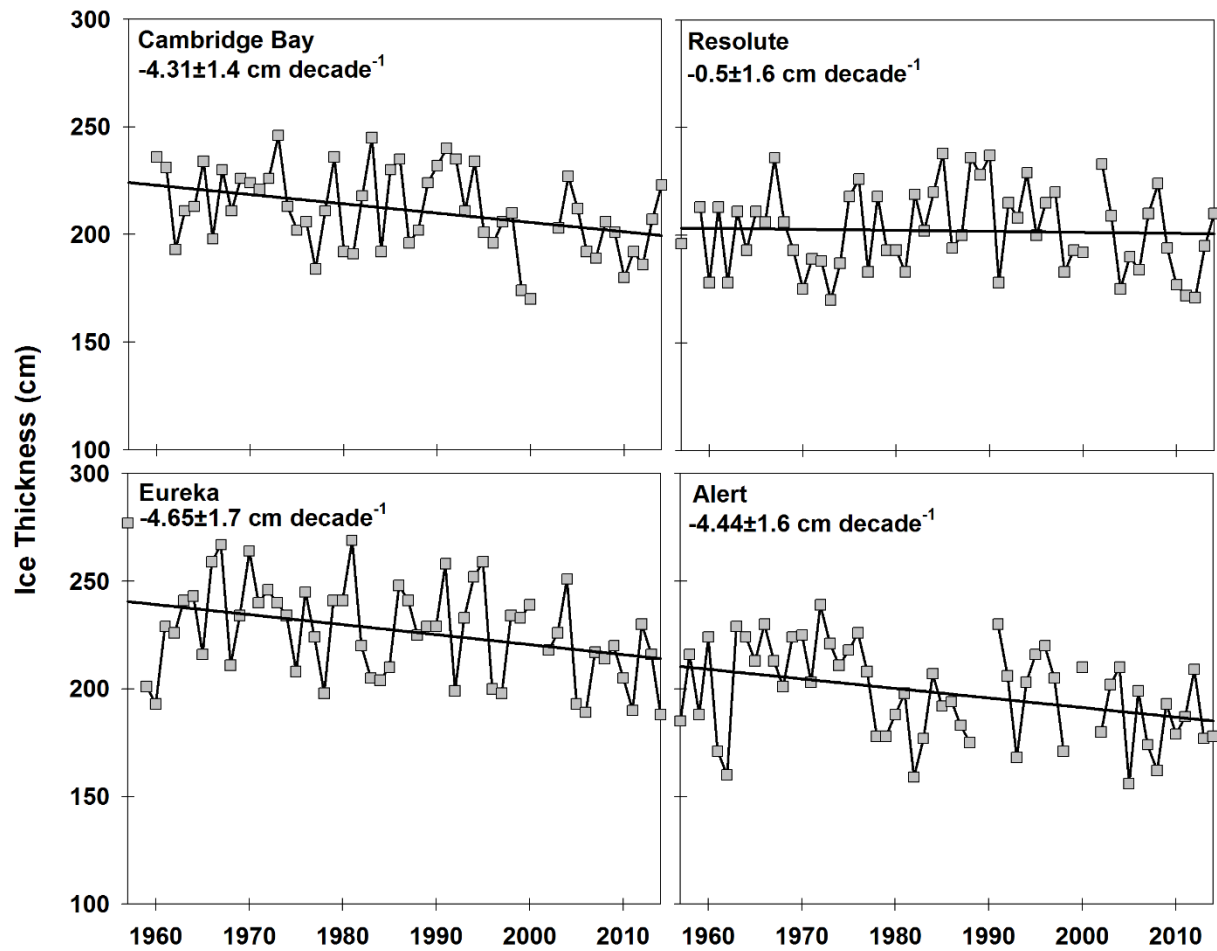
744
745 Figure 4. Time series and trend of observed maximum ice thickness at the four sites.
746
747
748
749
750
751
752
753
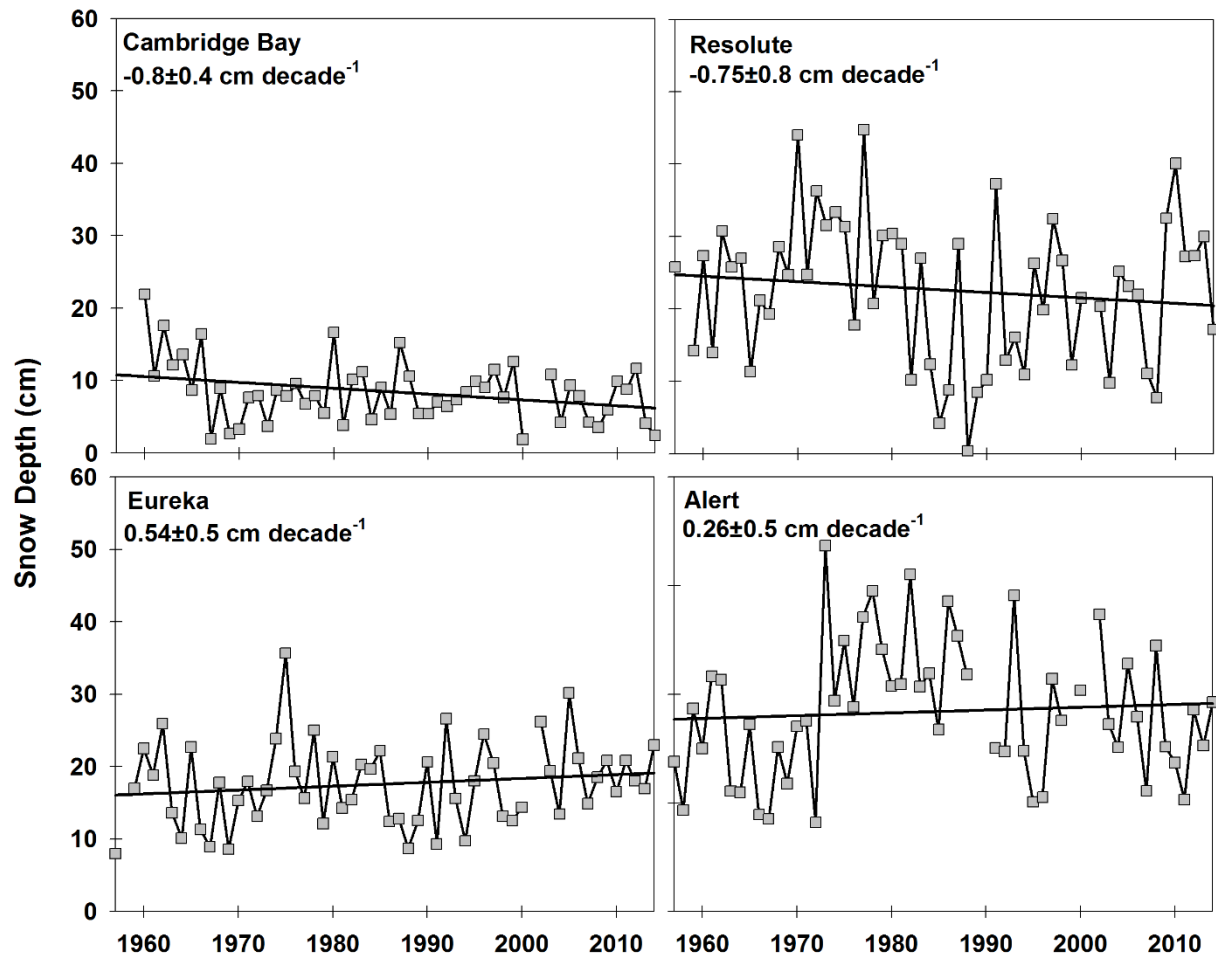
754
755 Figure 5. Time series and trend of observed mean October through May snow depth at the four
756 sites.
757
758
759
760
761
762
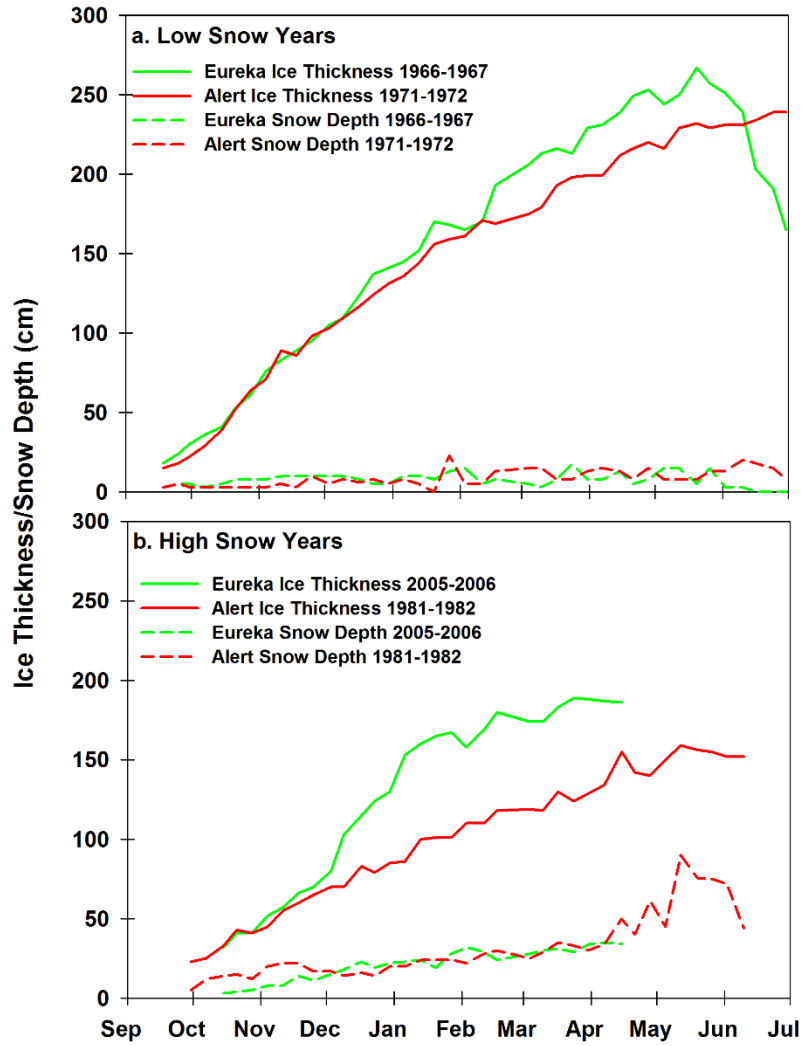
763
764    Figure 6. Weekly time series of ice thickness and snow depth at Eureka and Alert for (a) low
765    snow years and (b) high snow years.

766
767
768
769
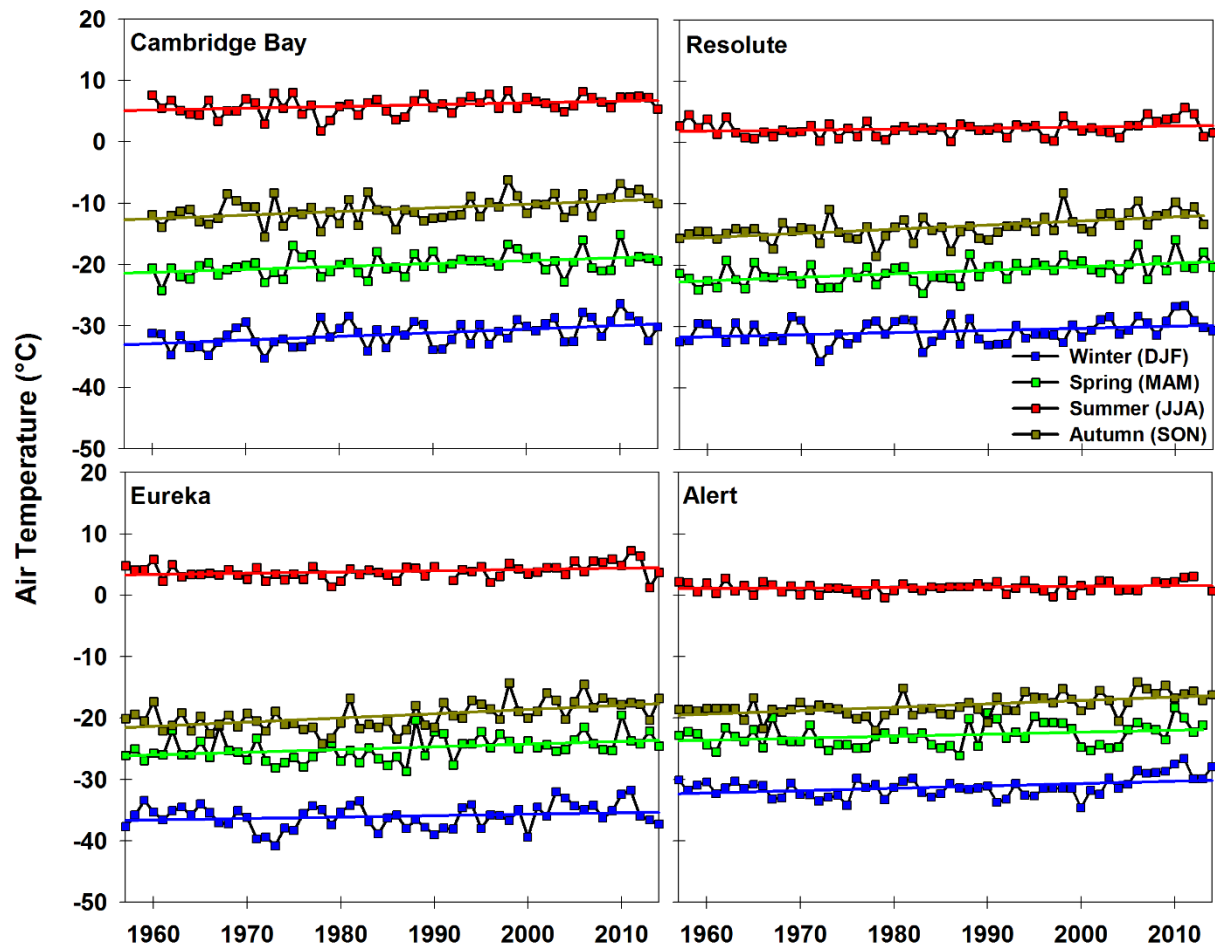
Figure 7. Time series observed mean air temperature by Environment Canada during winter (DFJ), spring, (MAM), summer (JJA) and autumn (SON) at the Cambridge Bay, Resolute, Eureka and Alert.
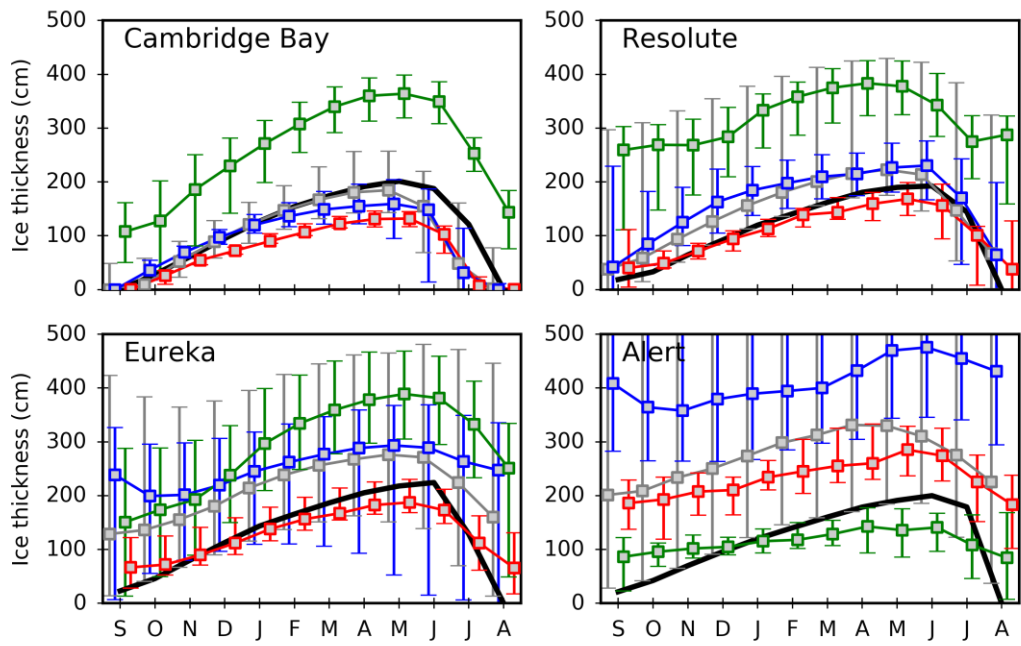
779
780    Figure 8. CMIP5 median sea ice thickness seasonal cycle (1955-2014) at stations (grey).
781    Observations from 2 (black). Median of ORA-IP models CGLORS, ORAP5.0, GLORYS2V3
782    (blue), ECCO-v4 (green) and UR025.4 (red). Whiskers indicate the 5th and 95th percentiles.
783
784
785
786
787

788
789
790 Figure 9. Same as Figure 8 for snow depth and only for CMIP5 models (grey) and observations
791 (black).
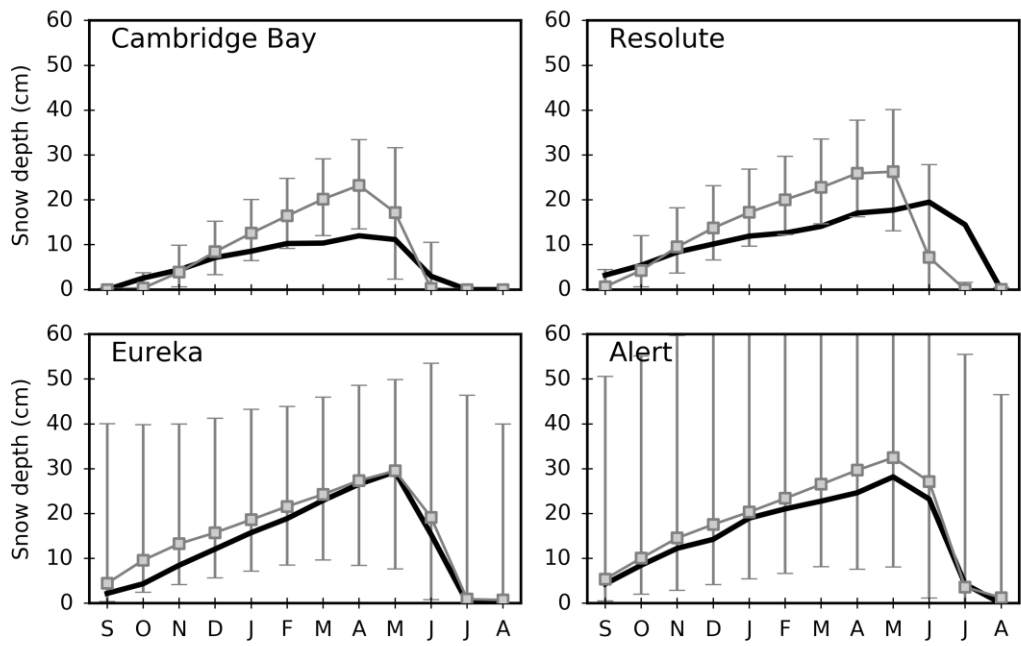
792
793
794
795
796
797
798
799
800
801
802
803
804
805
806
807
808
809
810
811
812
813
814
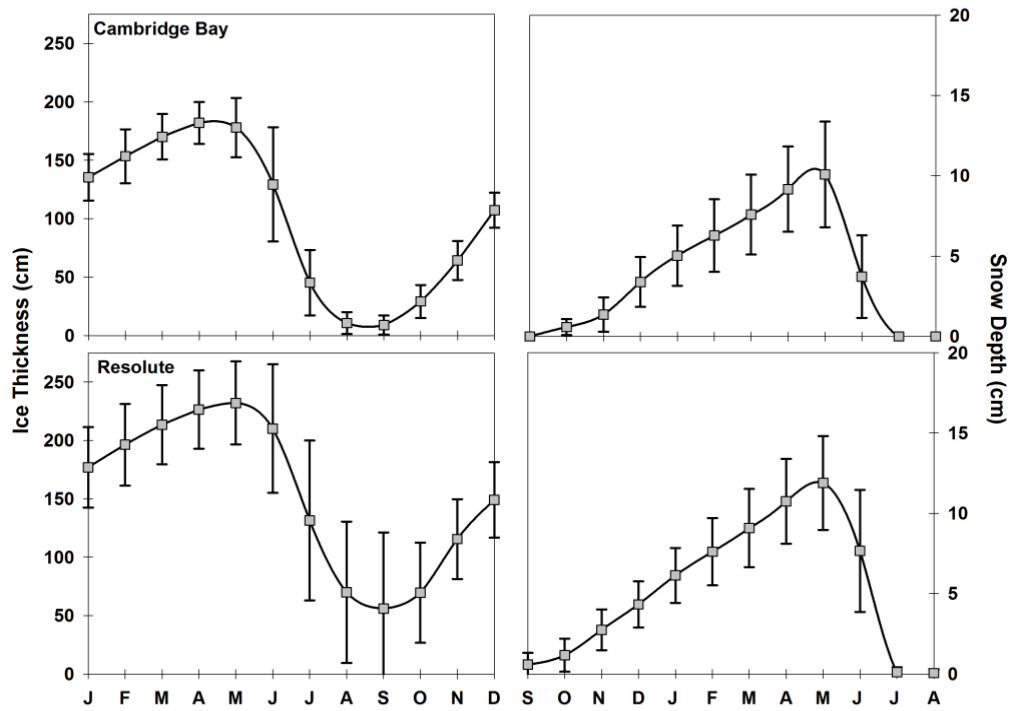
815
816 Figure 10. Seasonal cycle of observed mean ice thickness (left) and snow depth (right) from
817 PIOMAS at Cambridge Bay and Resolute (1979-2014).
818
819
820
821
822
823
824
825
826
827
828
829
830
831
832
833
834
835
836
837
838
839
840
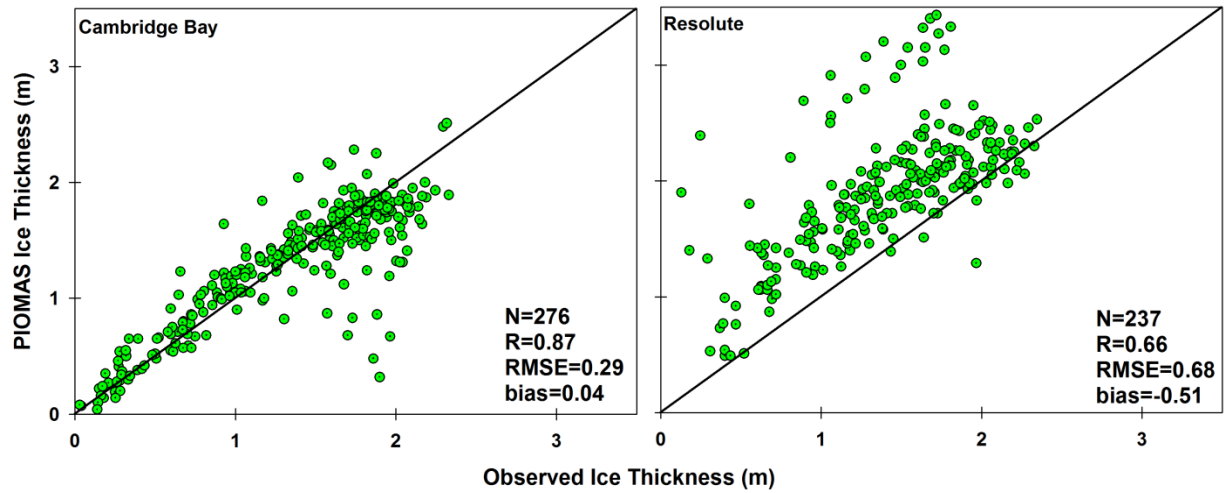
841
842  Figure 11. Comparison of PIOMAS ice thickness with ice thickness observations from
843  Environment Canada's ice thickness monitoring sites at Cambridge Bay and Resolute. The data
844  covers the period 1979-2014.
845
846
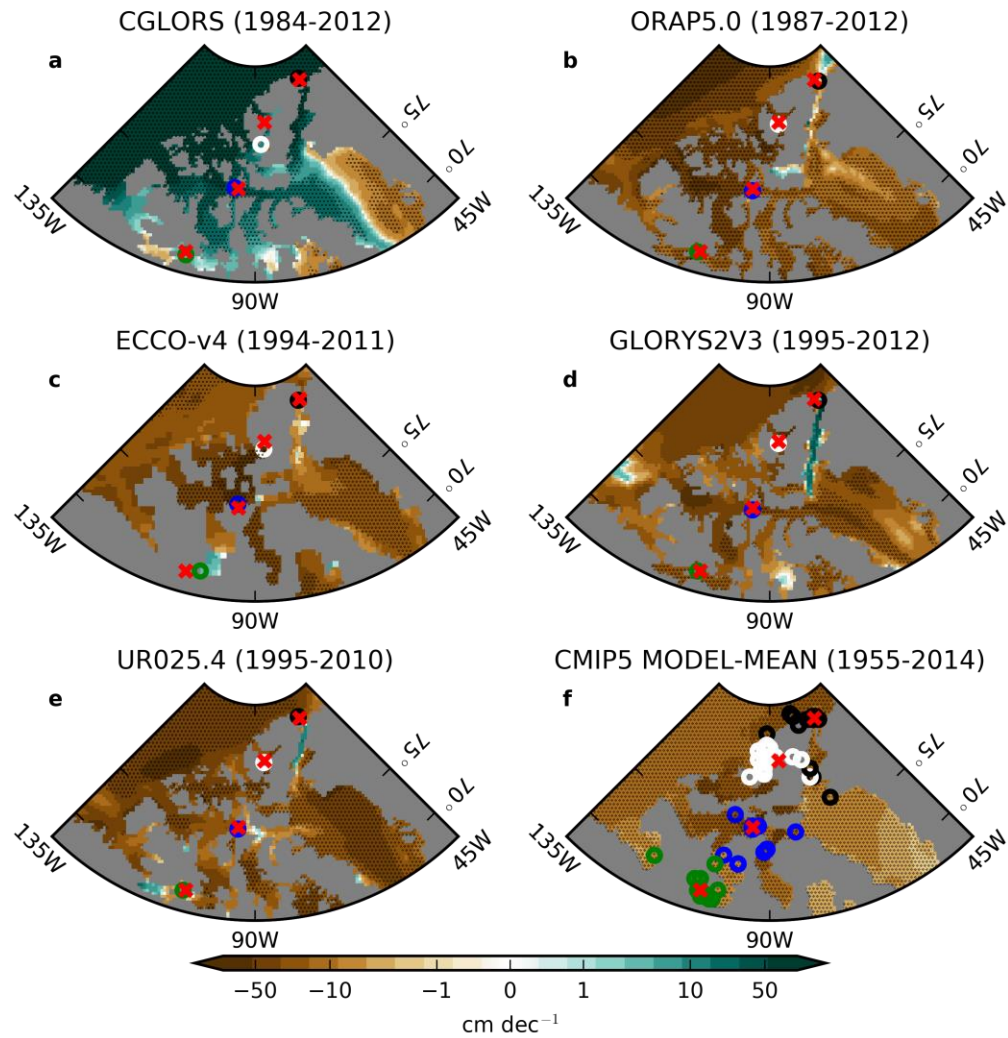
847
848 Figure 12. **a-e:** Maximum sea ice thickness trends in ORA-IP simulations. **f:** Same for CMIP5
849 MODEL-MEAN. From South to North, o's indicate Cambridge Bay (green), Resolute (blue),
850 Eureka (white) and Alert (black) and x's indicate the corresponding measurement stations. In f,
851 one o per model is shown." The stippling indicates p-values less than 0.05, corrected using the
852 False Discovery Rate (FDR) method with a global pFDR-values less than 0.10 [*Wilks*, 2006].
853 The colorbar is linear from -10 cm dec$^{-1}$ to 10 cm dec$^{-1}$ and symmetric logarithmic beyond these
854 values.
855
856
857
858
859
860
861
862
863
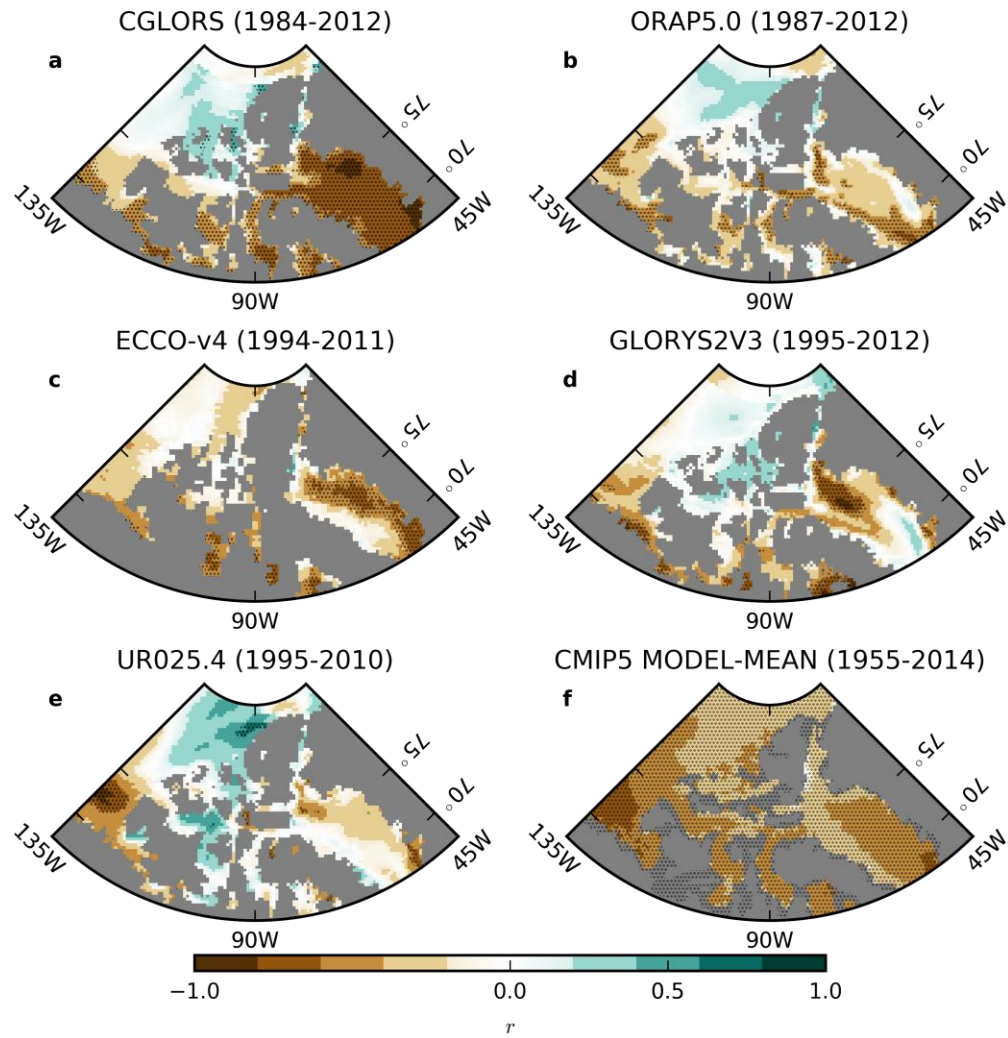
864
865 Figure 13. **a-e:** Pearson correlation of detrended maximum sea ice thickness in ORA-IP with
866 detrended ONDJFMAM ERA-INTERIM 2m temperature. **f:** Same but for CMIP5 MODEL-
867 MEAN. The stippling indicates p-values less than 0.05, corrected using the False Discovery Rate
868 (FDR) method with a global pFDR-values less than 0.10 [*Wilks*, 2006].
869
870
871
872
873
874
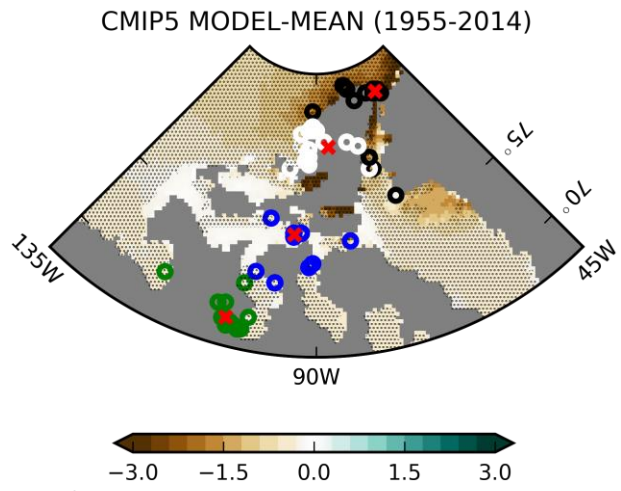
875
876    Figure 14. Same as Figure 12**f** but for snow depth trends (ONDFJMAM).